

UC Irvine

UC Irvine Previously Published Works

Title

Neuroimaging Findings of the Post-Treatment Effects of Radiation and Chemotherapy of Malignant Primary Glial Neoplasms

Permalink

<https://escholarship.org/uc/item/03m7c7h1>

Journal

The Neuroradiology Journal, 26(4)

ISSN

1120-9976

Authors

Mamlouk, MD
Handwerker, J
Ospina, J
et al.

Publication Date

2013-08-01

DOI

10.1177/197140091302600405

Peer reviewed

Neuroimaging Findings of the Post-Treatment Effects of Radiation and Chemotherapy of Malignant Primary Glial Neoplasms

M.D. MAMLOUK, J. HANDWERKER, J. OSPINA, A.N. HASSO

Department of Radiology, University of California; Irvine, Orange, CA, USA

Key words: radiation necrosis, recurrent tumor, pseudoprogression, pseudoresponse, leukoencephalopathy

SUMMARY – *Post-treatment radiation and chemotherapy of malignant primary glial neoplasms present a wide spectrum of tumor appearances and treatment-related entities. Radiologic findings of these post-treatment effects overlap, making it difficult to distinguish treatment response and failure. The purposes of this article are to illustrate and contrast the imaging appearances of recurrent tumor from necrosis and to discuss other radiologic effects of cancer treatments. It is critical for radiologists to recognize these treatment-related effects to help direct clinical management.*

Introduction

Imaging malignant primary glial neoplasms after cancer treatment poses a diagnostic dilemma due to the heterogeneity of treatment-related effects. To compound matters, the distinction between typical effects related to therapy and those of worsening or recurrent neoplasm is blurred. This results in a diagnostic conundrum that may delay diagnosis and subsequent management.

This article presents a spectrum of the neuroimaging findings related to radiation and chemotherapy of malignant primary glial neoplasms. The discussion will be limited to the intracranial findings—head and neck pathologies will not be addressed. Specific topics include (a) radiation necrosis versus recurrent tumor, (b) pseudoprogression and pseudoresponse, (c) nonenhancing tumor, (d) radiation-induced neoplasia, (e) white matter injury and leukoencephalopathy, and (f) vascular-related pathologies. This collage of entities will be depicted through computed tomography (CT) and magnetic resonance (MR) imaging, including advanced MR techniques such as perfusion, spectroscopy, and diffusion.

Radiation Necrosis, Tumor Recurrence, Radiation-Induced Neoplasia

Radiation Necrosis

The incidence of radiation necrosis after radiotherapy for brain tumors ranges from 3-24%¹. Radiation necrosis usually occurs approximately two to 32 months after radiotherapy, with 85% of cases occurring within two years². Earlier presentations of necrosis can be seen when there is combined radiation and chemotherapy³. The likelihood of radiation necrosis is related to both the volume of irradiated brain and the total radiation dose administered. With a total dose <45 Gy, 5% of patients may develop necrosis⁴, whereas the likelihood of necrosis markedly increases with a total dose >64.8 Gy⁵. Fractionated radiation, the administration of smaller doses over multiple attempts, is more commonly used to allow non-cancerous cells to recover^{2,6}.

Knowledge of the radiation technique and field are other important factors when evaluating patients with radiation necrosis. The modern intensity-modulated radiation therapy technique is commonly used because it provides the best tradeoff of tumor dose with

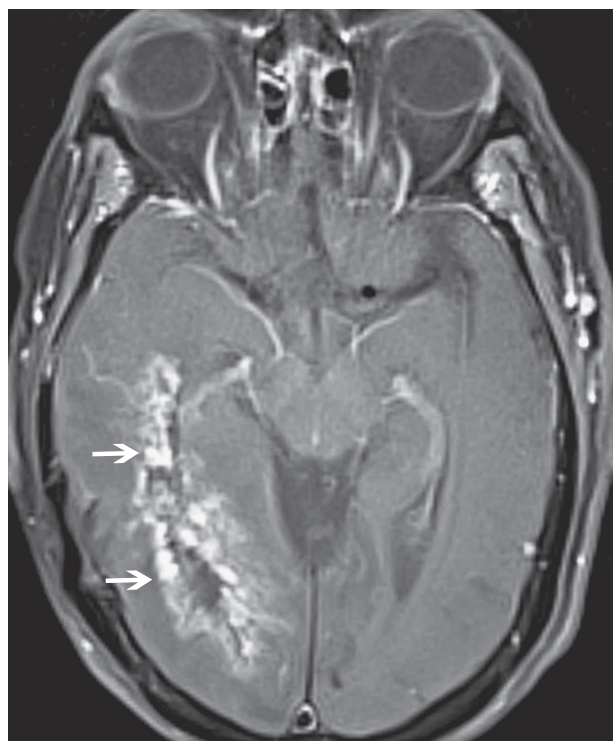


Figure 1 Radiation necrosis in a 73-year-old woman after radiation therapy for astrocytoma. Axial contrast-enhanced fat-saturated T1-weighted MR image shows an enhancing periventricular lesion with a “Swiss cheese” configuration (arrows).

relative sparing of normal tissues. Stereotactic radiation therapy delivers radiation with the guidance of fiducial markers. Radiosurgery, a type of stereotactic therapy performed with gamma knife, delivers a single fraction of radiation. While a complete overview of the various radiotherapy techniques is beyond the scope of this article, acknowledging the specific type of radiotherapy used in each patient is essential to characterize radiation necrosis on imaging.

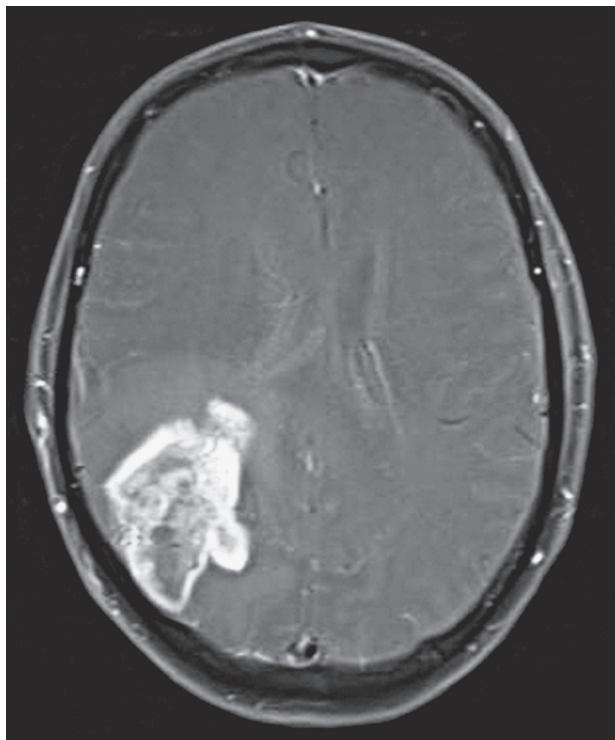
The exact pathogenesis of radiation-induced toxicity is not fully understood, but includes a combination of proposed mechanisms: vascular injury, glial and white matter damage, and

altering the fibrinolytic enzyme and immune systems⁷. Radiation-induced endothelial cell apoptosis is a common pathway that leads to disruption of the blood-brain barrier—the hallmark explanation for enhancement and surrounding edema in radiation necrosis^{8,9}.

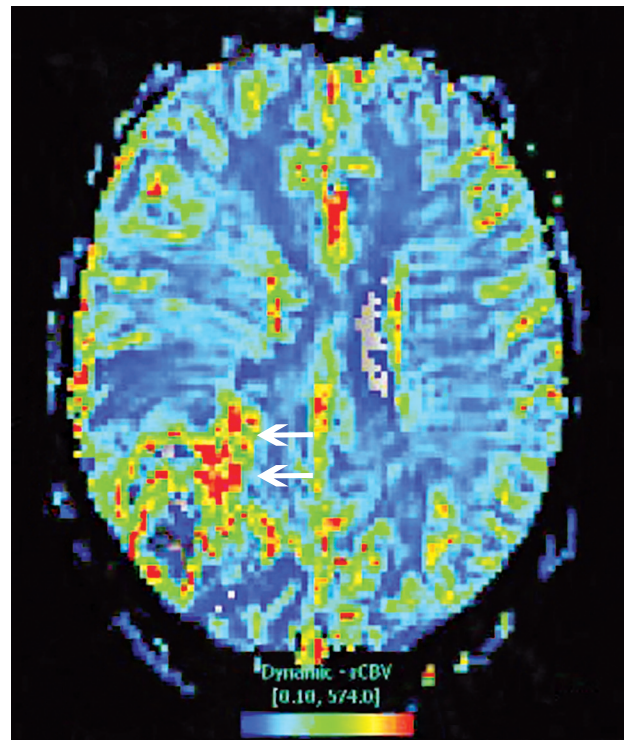
Radiation necrosis most commonly appears at the original tumor location—the site of maximum radiation delivery. Radiation necrosis usually consists of a single lesion; however, multiple lesions can arise, albeit less commonly. Periventricular white matter is the most common site of radiation injury, possibly due to a poor blood supply that produces ischemia^{10,11}.

Table 1 MR characteristics of post-treatment radiation necrosis and tumor.

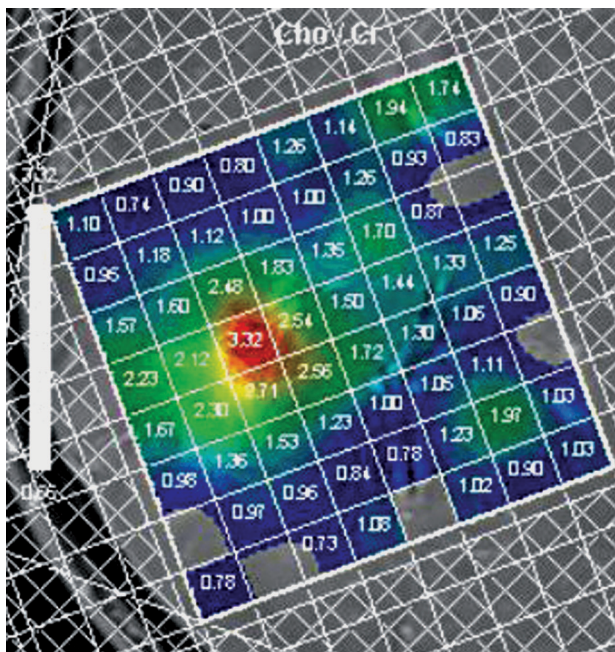
Entity	Sequence					
	T1C	T2	DSC MR Perfusion	MR Spectroscopy	DWI	Notable comments
Radiation Necrosis	↑	↑	↓ rCBV	Variable Cho/Cr ↓ Cho/NAA ↑ Lipids	Variable/↓	“Swiss cheese-like” enhancement
Recurrent Tumor	↑	↑	↑ rCBV	↑ Cho/Cr ↑ Cho/NAA	Variable/↑	Multiple lesions, cross midline
Pseudoprogression	↑→↓	↑→↓	↓ rCBV/ Variable	Variable	Variable	Follow-up imaging important
Pseudoresponse	↓→↑	↓→↑	↓ rCBV/ Variable	Variable	Variable	Follow-up imaging important; occurs with anti-angiogenic drugs



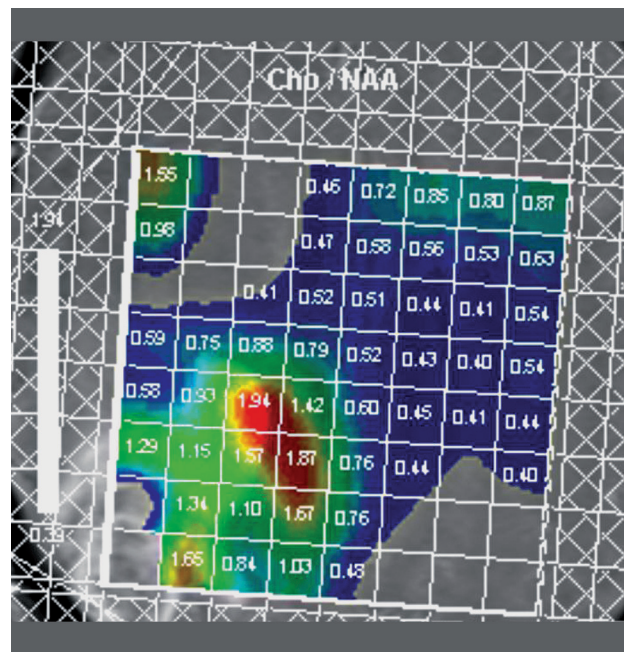
A



B

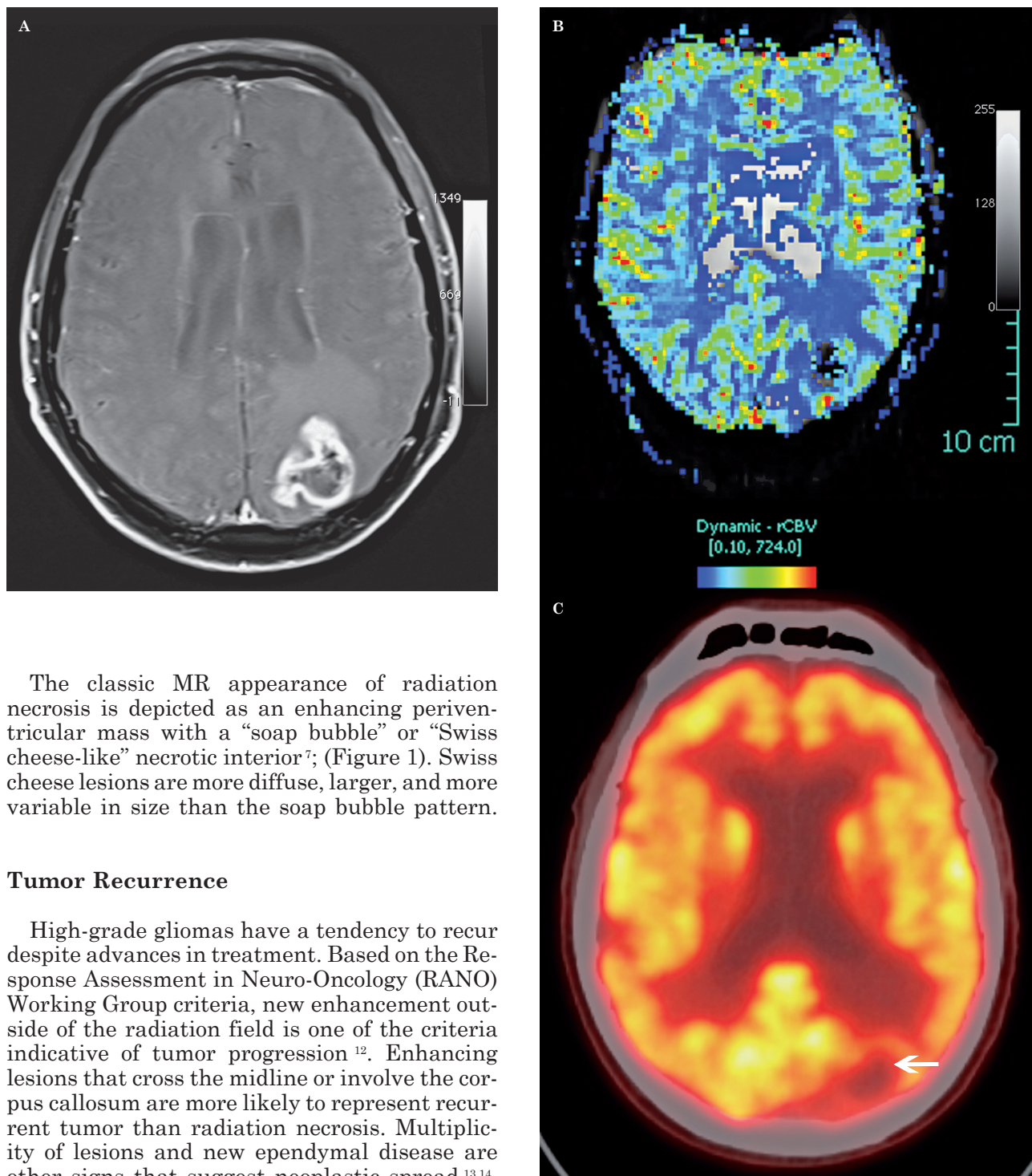


C



D

Figure 2 Recurrent glioblastoma multiforme in a 51-year-old man after radiation therapy. A) Axial contrast-enhanced fat-saturated T1-weighted MR image shows a large enhancing necrotic mass centered in the right parietal lobe. B) DSC perfusion MR image shows increased rCBV in the anteromedial aspect of the lesion compatible with recurrent tumor (arrows). C,D) MR multi-voxel spectroscopy maps (TE=144 milliseconds) show a Cho/Cr peak ratio of 3.32 (C) and a Cho/NAA peak ratio of 1.94 (D) in the same anteromedial region compatible with recurrent tumor.



The classic MR appearance of radiation necrosis is depicted as an enhancing periventricular mass with a “soap bubble” or “Swiss cheese-like” necrotic interior⁷; (Figure 1). Swiss cheese lesions are more diffuse, larger, and more variable in size than the soap bubble pattern.

Tumor Recurrence

High-grade gliomas have a tendency to recur despite advances in treatment. Based on the Response Assessment in Neuro-Oncology (RANO) Working Group criteria, new enhancement outside of the radiation field is one of the criteria indicative of tumor progression¹². Enhancing lesions that cross the midline or involve the corpus callosum are more likely to represent recurrent tumor than radiation necrosis. Multiplicity of lesions and new ependymal disease are other signs that suggest neoplastic spread^{13,14}.

Despite these useful tips and criteria, non-specific enhancement in a single lesion within the radiation field is more common and this poses a diagnostic dilemma—non-specific enhancement may represent recurrent tumor, radiation necrosis, or the combination. Moreover, even the aforementioned classic appearances of radiation necrosis do not reliably differentiate

Figure 3 Radiation necrosis in an 86-year-old man after radiation therapy for high-grade glioma. A) Axial contrast-enhanced fat-saturated T1-weighted MR image shows an irregular enhancing mass in the left parietal lobe. B) DSC perfusion MR image shows low rCBV in the lesion (arrow). C) Fused PET-CT with 2-[fluorine-18] fluoro-2-deoxy-D-glucose shows focal decreased glucose metabolism in the lesion (arrow). PET-CT is an additional imaging modality in the radiologist’s armamentarium, but the definitiveness of differentiating necrosis or recurrent tumor is not always straightforward.

necrosis from tumor¹⁵. Positron emission tomography (PET) has been used as an adjunct to help answer this clinical question, but with mixed results^{16,17}. Because of these equivocal conventional MR and PET findings, advanced MR techniques such as perfusion, spectroscopy, and diffusion have been researched in efforts to lessen this diagnostic dilemma. These advanced MR techniques will be discussed in detail henceforth (Table 1).

Dynamic Susceptibility Contrast MR Perfusion

Dynamic susceptibility contrast (DSC) MR perfusion has played a significant role in differentiating recurrent tumor and radiation necrosis^{14,18-23}. The rationale for DSC MR perfusion is that recurrent tumors have a greater blood supply secondary to neo-angiogenesis compared to radiation-induced necrotic brain. Relative cerebral blood volume (rCBV) is the primary DSC MR perfusion parameter and is measured by placing a region of interest over the enhancing lesion. A second region of interest is placed in the contralateral white matter, at approximately the same location, to establish a control cerebral blood volume. Attention is made to avoid susceptibility artifacts, partial volume effects, and vasculature when drawing the regions of interest. DSC MR perfusion shows that tumors have a higher rCBV than the control cerebral blood volume²⁰; (Figure 2). This is in contrast to a smaller rCBV between radiation necrosis and the control (Figure 3). Absolute rCBV cutoffs between tumor and necrosis have not been established, but an rCBV greater than 2.6 and an rCBV less than 0.6 were suggestive of recurrent tumor and nonneoplastic contrast-enhancing tissue, respectively²². rCBV is useful to distinguish tumor and necrosis; however, overlapping rCBV values can occur²⁰. T2*-weighted relative peak height and percentage of signal intensity recovery, the latter being a marker of capillary permeability, are two other MR perfusion parameters that also have been shown to be accurate indicators of recurrent tumor, and may be less prone to measurement overlap between the two entities²⁰. Lastly, arterial spin labeling is another alternative in MR perfusion analysis instead of DSC²⁴.

MR Spectroscopy

MR spectroscopy attempts to identify tumor recurrence on a biochemical level. Tumor recurrence is characterized by high ratios of choline/

creatine (Cho/Cr) and choline/N-acetylaspartate (Cho/NAA) (Figure 2). Radiation necrosis shows elevated lactate and lipid peaks. Despite these characteristics, there has been conflicting literature on the success of MR spectroscopy to distinguish recurrent tumor from radiation injury²⁵. A major problem in comparing different studies on MR spectroscopy is the use of various methods to calculate metabolite ratios²⁵. Another pitfall is due to similar metabolite peaks with radiation-injured brain, such as decreased NAA²⁵. Lesions close to the ventricular system or skull yield unreliable measurements due to magnetic susceptibility artifact²⁰. Lastly, the use of single versus multiple voxel spectroscopy has produced conflicting data.

Fink et al. showed multiple voxel spectroscopy to be superior to the single voxel technique. Single voxel spectroscopy suffers from volume averaging, the uncertainty of ideal voxel location, and the possibility of selection bias¹⁹. This group showed that multi-voxel techniques were statistically reliable to detect recurrent tumor. A multi-voxel Cho/Cr peak-area >1.54 and Cho/NAA peak height >1.05 had 93.1% and 89.7% accuracies for recurrent tumor, respectively. Similar findings were seen in another study that also used multiple voxel spectroscopy²⁶. While more research is needed to validate results, initial data on multiple voxel spectroscopy are promising to differentiate recurrent tumor from radiation-related changes.

Diffusion-Weighted Imaging

Diffusion-weighted imaging (DWI) has been studied to differentiate recurrent tumor and necrosis. Originally, the two premises of DWI concerning tumor were: (a) highly cellular tumors show reduced diffusion, and (b) apparent diffusion coefficient (ADC) values are lower in recurrent tumor than radiation necrosis²⁷. However, these observations have pitfalls. DWI and ADC show heterogeneous signal intensities due to variable tumor cellularity, as well as regions of mixed tumor and necrosis. ADC values in recurrent tumor are not consistent—low or high ADC values may be seen²⁸. In addition, inflammatory processes, such as radiation-induced inflammation, are often present and may cause altering signal effects. Thus, ADC does not always provide definitive information with regard to the presence of recurrent tumor, but recent research shows ADC may provide a more adjunctive role. Pope et al. found that ADC histogram analysis of MR im-

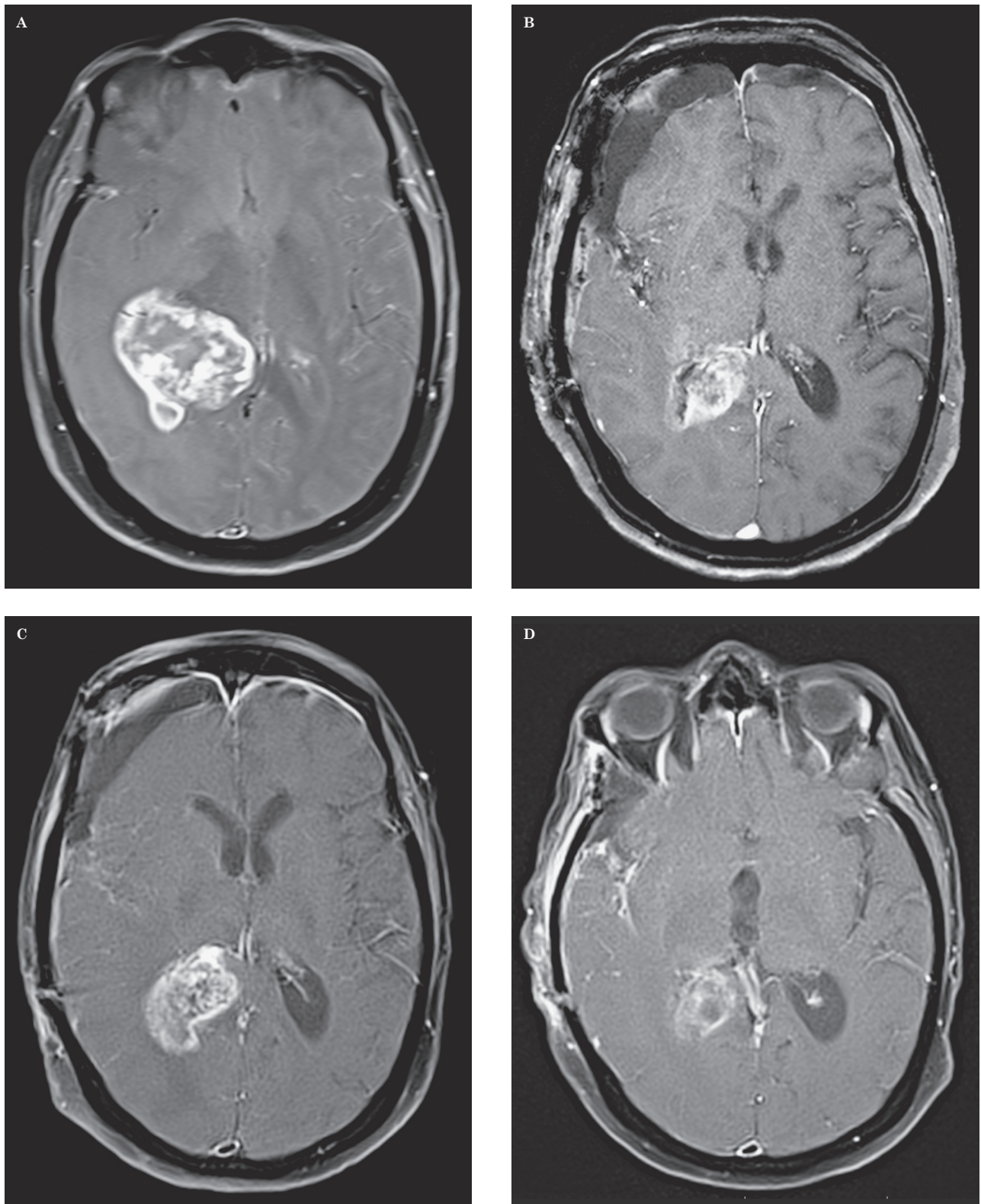


Figure 4 Pseudoprogression in a 68-year-old woman with glioblastoma multiforme. A-D) Axial contrast-enhanced fat-saturated T1-weighted MR images show a large enhancing mass centered in the right thalamus prior to treatment (A), immediately postoperative (B), two months later with increased contrast enhancing tumor after temozolomide chemoradiotherapy (C), and one month later with decreased tumor enhancement (D). T2-weighted images (not shown) demonstrated peri-tumoral vasogenic edema that followed the same patterns as contrast enhancement.

ages prior to bevacizumab treatment (Avastin [Genentech, South San Francisco, CA, USA]) for glioblastoma was 72.5% accurate in stratifying six-month progression-free survival²⁹.

Comparing the efficacy of these advanced MR techniques for discerning recurrent tumor between post-treatment changes, Fink et al. compared the use of 3T MR spectroscopy, perfusion, and diffusion in 40 intracranial lesions (38 patients). The reference standard was both surgical biopsy (14/40) and extensive follow-up imaging (26/40). They concluded that MR perfusion and multiple voxel spectroscopy outperformed DWI for distinguishing recurrent glioma from post-treatment effects¹⁹. Despite this study, there are currently no absolute noninvasive parameters to distinguish recurrent tumor from radiation necrosis. It is also important to mention that the answer to this conundrum may not always simply be a dichotomy of tumor or radiation necrosis, but often a combination is present. As detailed, many of the conventional and advanced MR techniques have relative strengths and weaknesses. However, the combination of these MR techniques will likely provide the best noninvasive accurate diagnosis currently available².

Pseudoprogression

Pseudoprogression is characterized by transient increased tumor enhancement followed by a subsequent decrease or stabilization without any further treatment. Pseudoprogression may be misinterpreted as tumor progression based on the classic MacDonald criteria that specify that tumor progression is likely to have occurred when the contrast-enhancing lesion has increased by >25%³⁰. With the advent of novel oncologic treatments, the presence or lack of contrast enhancement has not been shown to be a reliable marker of progression or response, respectively, but rather a sign of a disrupted blood-brain barrier seen with pseudoprogression and pseudoresponse.

Pseudoprogression has occurred most notably with the addition of temozolomide to radiotherapy in the management of glioblastoma. It can occur in up to 30% of patients treated with temozolomide chemoradiotherapy, and may occur two to six months after chemoradiotherapy^{1,14,31,32}. This treatment-related effect has important implications for patient management and may result in cessation of effective therapy if misconstrued as true tumor progression. In

fact, pseudoprogression has been shown to result in improved overall survival³³, thus correct diagnosis is important.

The mechanism of pseudoprogression has not been fully elucidated, but it is likely that chemoradiotherapy damages tumor and endothelial cells. This results in increased edema and abnormal vessel permeability, which mimic tumor progression³⁴.

Conventional MR findings show increased tumor enhancement and edema due to an altered blood-brain barrier. On subsequent imaging, without additional chemoradiotherapy cycles, if the tumor enhancement decreases or stabilizes, this is a sign of pseudoprogression and a favorable marker of treatment response (Table 1; Figure 4). In contrast, if the majority of new enhancement is outside the radiation field, either within or after the first 12 weeks of chemoradiotherapy, the RANO criteria classify this enhancement as true tumor progression¹². Additional criteria defining progressive disease before and after 12 weeks of chemoradiotherapy are mentioned in the RANO criteria¹².

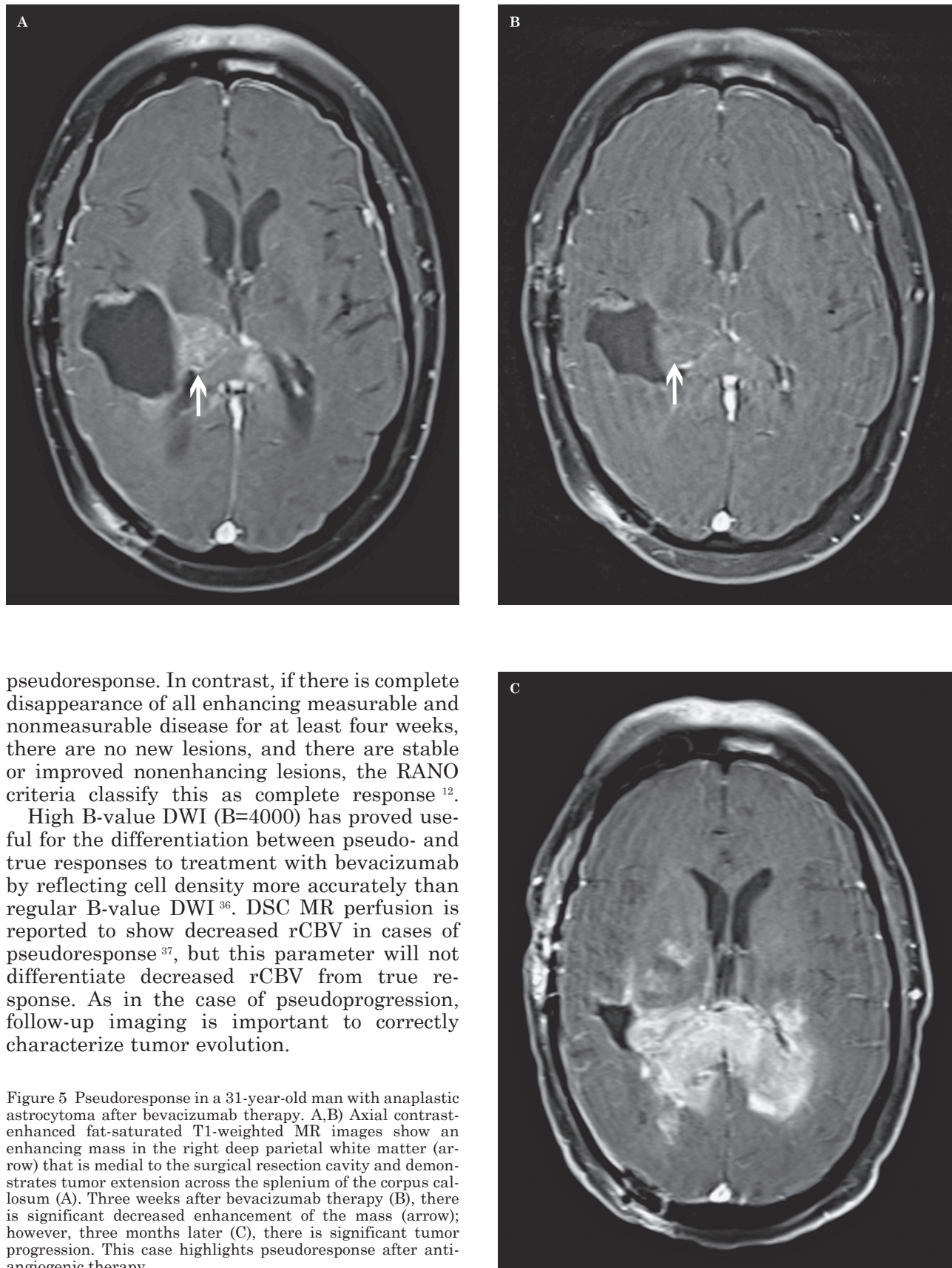
DSC MR perfusion may show decreased rCBV in cases of pseudoprogression³⁵. MR spectroscopy and DWI characteristics are variable to differentiate pseudoprogression from true progression³⁵.

Pseudoresponse

Pseudoresponse is virtually the opposite of pseudoprogression. Pseudoresponse is characterized by interval-reduced tumor enhancement after anti-angiogenic chemotherapy. This would suggest treatment response by the MacDonald criteria, but this reduced enhancement may not always indicate a favorable response.

Anti-angiogenic agents such as bevacizumab inhibit vascular endothelial growth factor (anti-VEGF) via the tyrosine kinase pathway. This vascular inhibition results in decreased contrast enhancement due to a "normalization" of the abnormally permeable blood-brain barrier. Results may occur as early as hours after therapy³⁴. Pseudoresponse has also been seen in patients that restarted anti-angiogenic therapy after taking a "drug holiday" due to symptomatic effects from drug toxicity³³.

MR findings show progressive reduction in tumor enhancement and edema soon after anti-angiogenic chemotherapy (Table 1; Figure 5). If the reduction in tumor enhancement is not maintained for four weeks, this is compatible with



pseudoresponse. In contrast, if there is complete disappearance of all enhancing measurable and nonmeasurable disease for at least four weeks, there are no new lesions, and there are stable or improved nonenhancing lesions, the RANO criteria classify this as complete response¹².

High B-value DWI (B=4000) has proved useful for the differentiation between pseudo- and true responses to treatment with bevacizumab by reflecting cell density more accurately than regular B-value DWI³⁶. DSC MR perfusion is reported to show decreased rCBV in cases of pseudoresponse³⁷, but this parameter will not differentiate decreased rCBV from true response. As in the case of pseudoprogression, follow-up imaging is important to correctly characterize tumor evolution.

Figure 5 Pseudoresponse in a 31-year-old man with anaplastic astrocytoma after bevacizumab therapy. A,B) Axial contrast-enhanced fat-saturated T1-weighted MR images show an enhancing mass in the right deep parietal white matter (arrow) that is medial to the surgical resection cavity and demonstrates tumor extension across the splenium of the corpus callosum (A). Three weeks after bevacizumab therapy (B), there is significant decreased enhancement of the mass (arrow); however, three months later (C), there is significant tumor progression. This case highlights pseudoresponse after anti-angiogenic therapy.

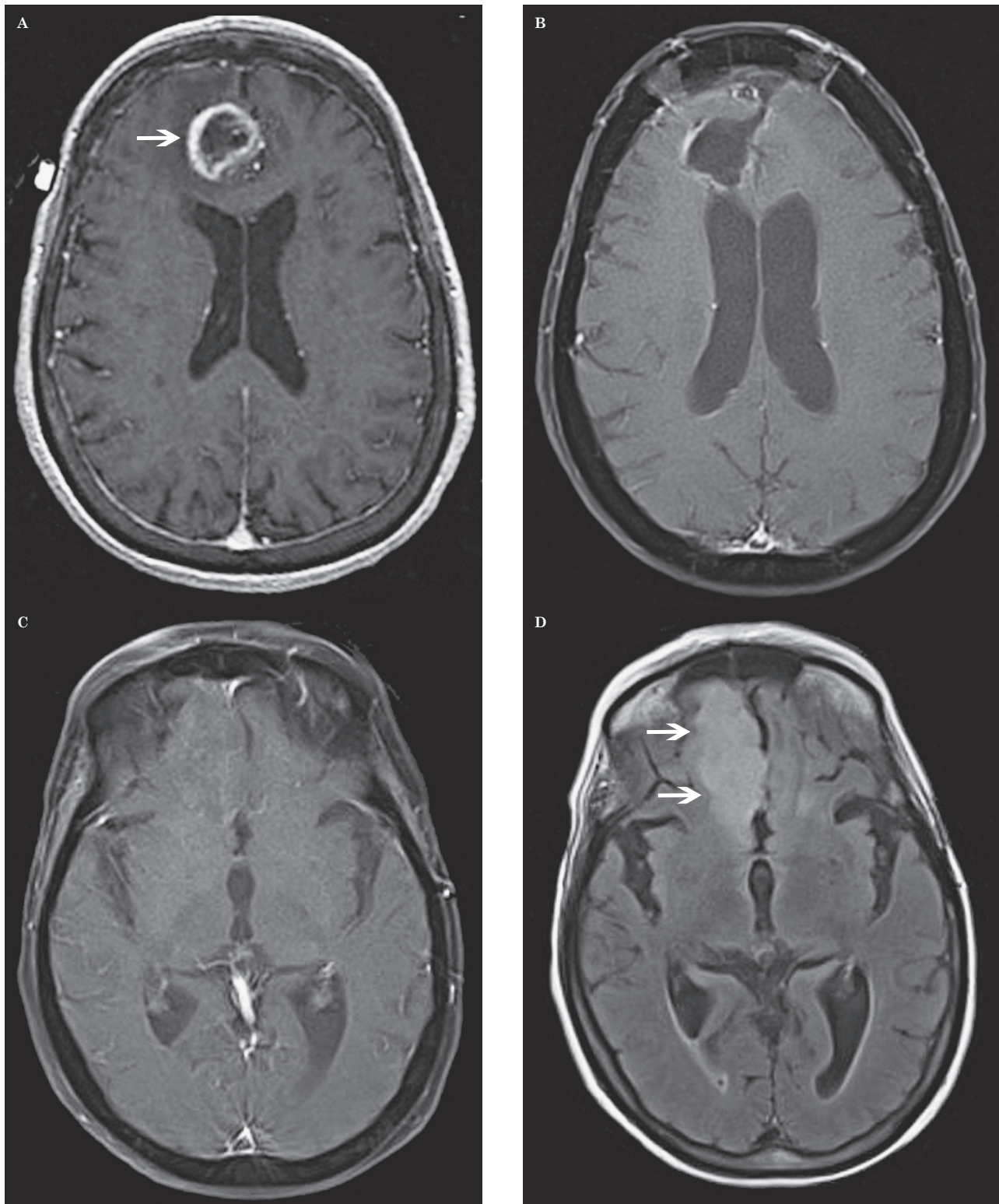


Figure 6 Nonenhancing tumor progression in a 74-year-old man with glioblastoma multiforme after bevacizumab therapy. A) Axial contrast-enhanced T1-weighted MR image shows a peripherally enhancing mass in the right medial frontal gyrus (arrow). B) Axial contrast-enhanced fat-saturated T1-weighted MR image shows a cavity after surgical resection. C) Axial contrast-enhanced fat-saturated T1-weighted MR image one year later after surgical resection does not show any enhancing lesion to suggest recurrence; however, (D) axial FLAIR MR imaging shows new high signal (arrows) in the right gyrus rectus (more inferior than the original tumor site) compatible with nonenhancing tumor.

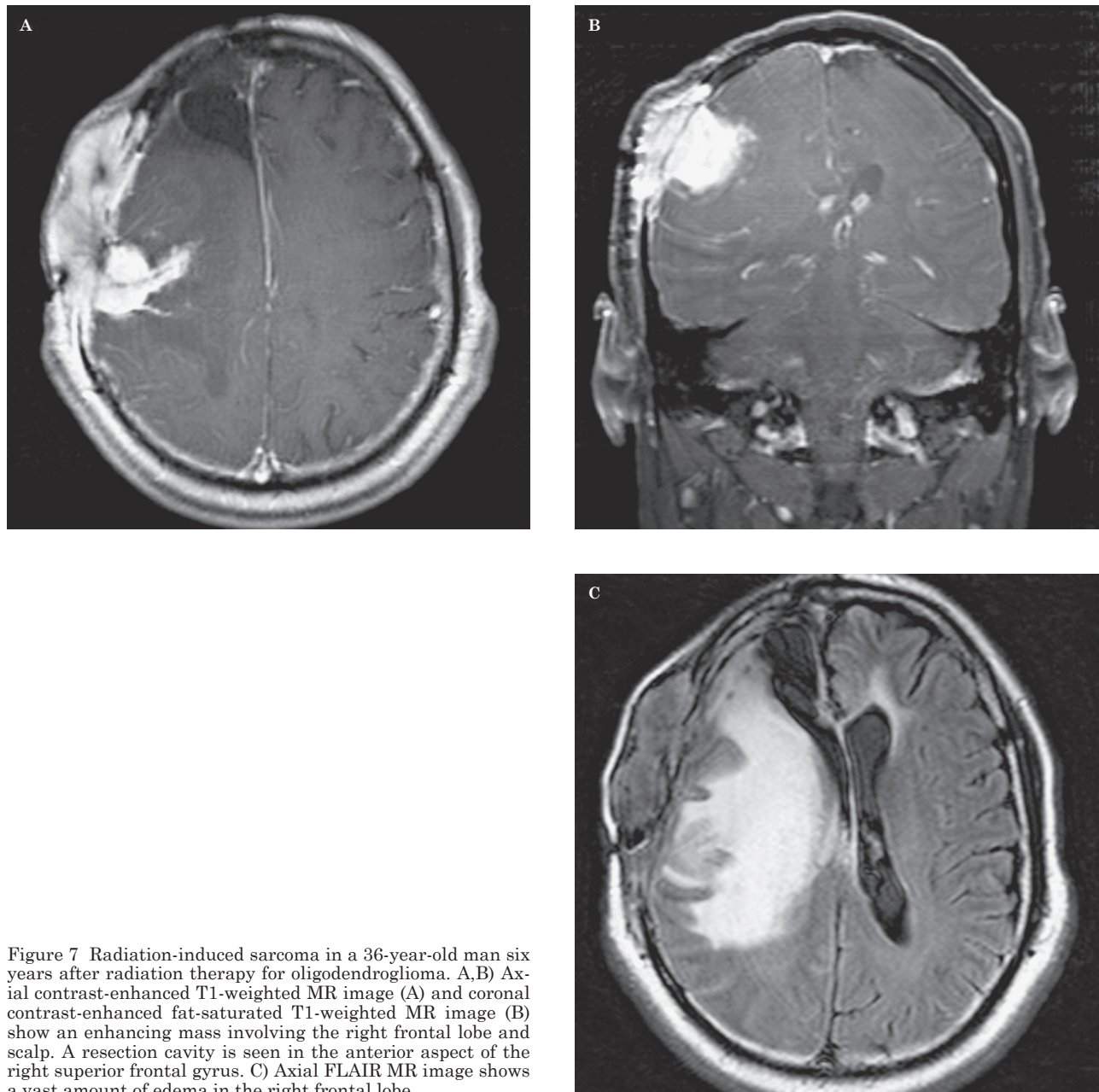


Figure 7 Radiation-induced sarcoma in a 36-year-old man six years after radiation therapy for oligodendroglioma. A,B) Axial contrast-enhanced T1-weighted MR image (A) and coronal contrast-enhanced fat-saturated T1-weighted MR image (B) show an enhancing mass involving the right frontal lobe and scalp. A resection cavity is seen in the anterior aspect of the right superior frontal gyrus. C) Axial FLAIR MR image shows a vast amount of edema in the right frontal lobe.

Nonenhancing Tumor

High-grade gliomas may not always disrupt the blood-brain barrier and cause enhancement due to their infiltrative nature. In addition, as mentioned, anti-angiogenic chemotherapy may cause decreased tumoral enhancement without true tumor reduction, making careful analysis of nonenhancing tumor essential¹². Increased nonenhancing tumor burden on T2-weighted imaging after anti-angiogenic therapy has been theorized to occur via the “vessel co-op-

tion” route, in which tumor dissemination is re-routed to another pathway secondary to the angiogenesis inhibition from chemotherapy³⁸. The RANO criteria define progression of non-enhancing tumor when a lesion shows a significant increase in T2/FLAIR signal while on stable or increasing doses of corticosteroids compared with the baseline scan¹²; (Figure 6). It is important to differentiate T2/FLAIR signal related to tumor from treatment-related effects such as demyelination, leukoencephalopathy, and ischemic injury.

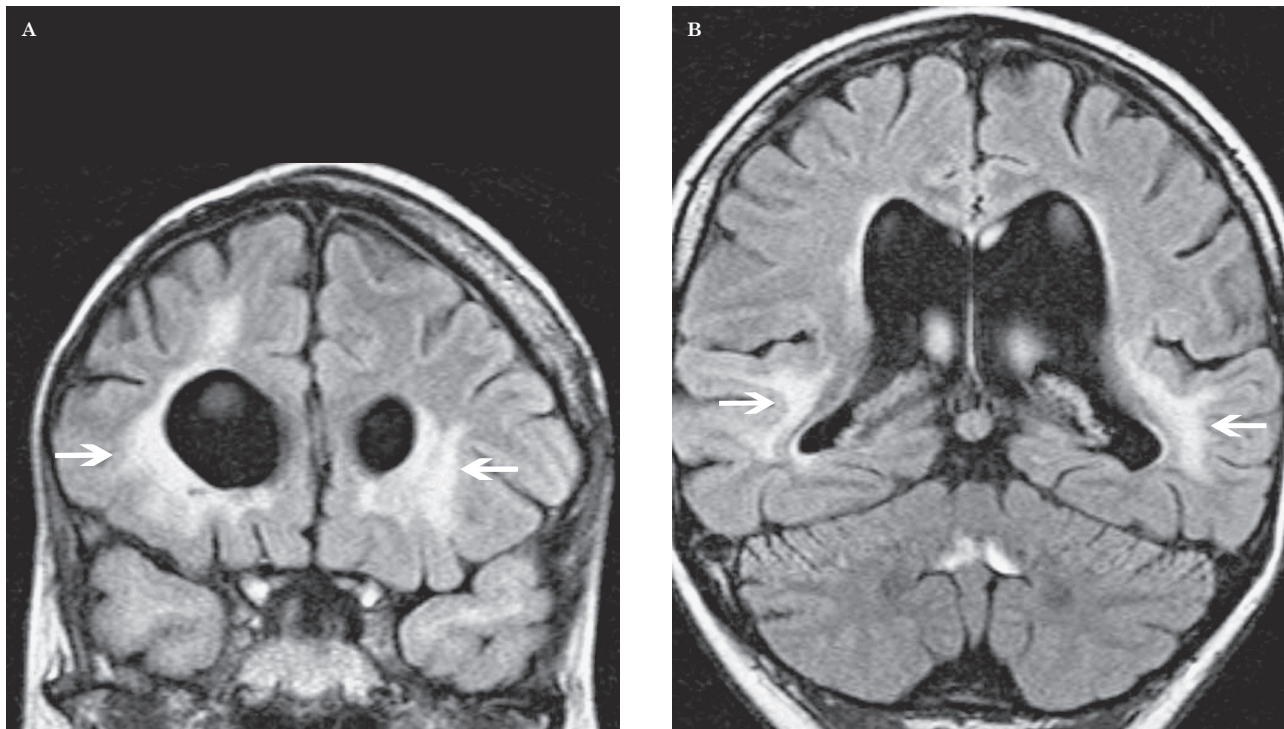


Figure 8 Diffuse white matter injury in a 29-year-old man 20 years after chemoradiotherapy for childhood optic glioma. A,B) Coronal FLAIR MR images at the levels of the frontal (A) and temporal horns (B) show periventricular high signal (arrows).

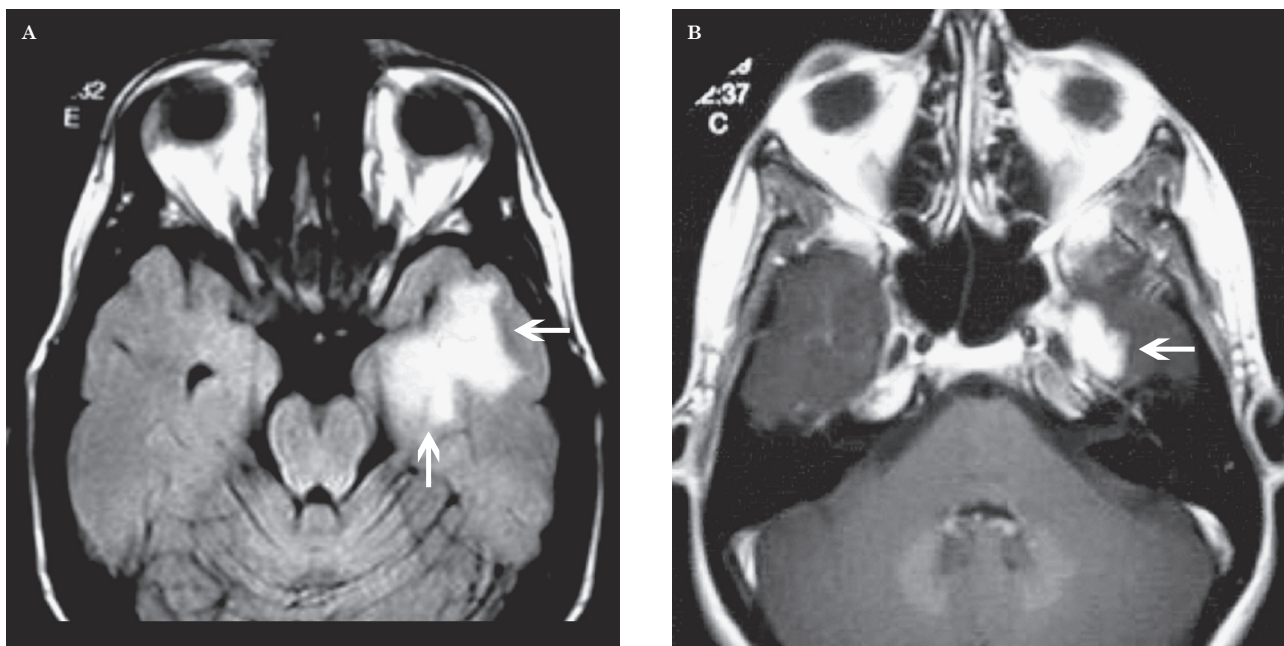


Figure 9 Temporal lobe injury after gamma knife radiosurgery for nasopharyngeal carcinoma. A) Axial FLAIR MR image shows a large amount of high signal in the left temporal lobe (arrows). B) Axial contrast-enhanced T1-weighted MR image more inferiorly shows enhancement (arrow) of the left temporal lobe in a smaller area relative to the high signal in (A). Both of these findings can spontaneously resolve.

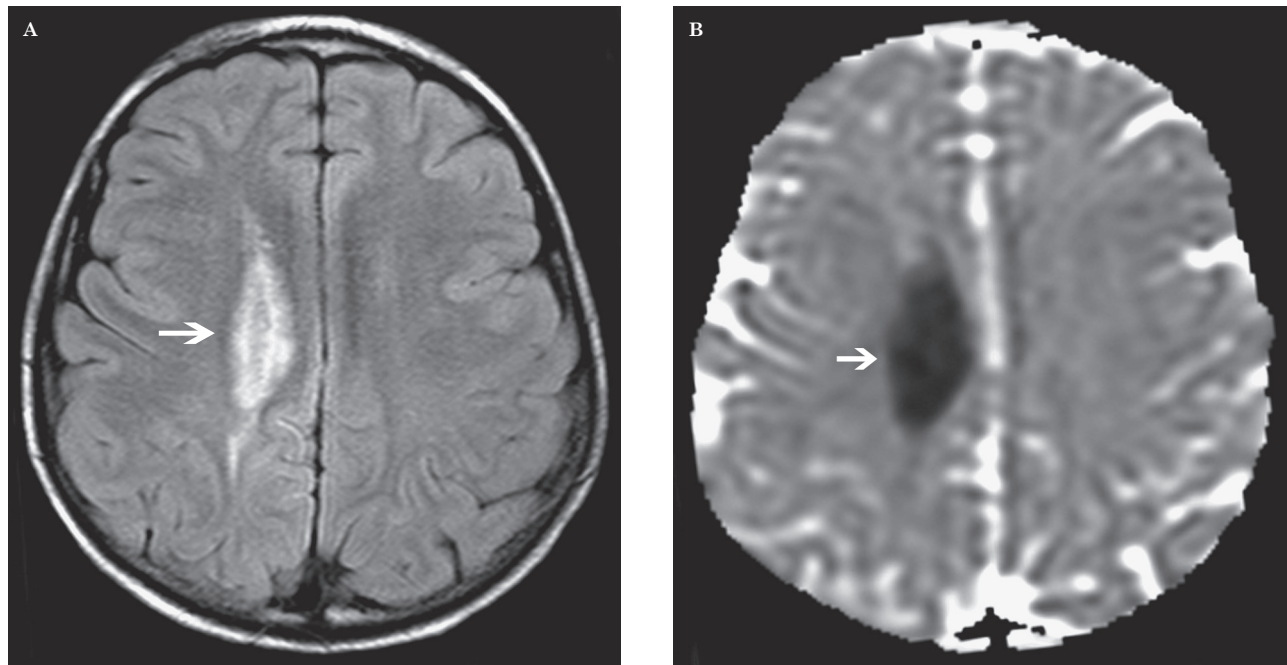


Figure 10 White matter injury in a 7-year-old boy after methotrexate. A) Axial FLAIR image shows high signal in the right centrum semiovale (arrow). B) Axial ADC MR image shows low signal (arrow) compatible with reduced diffusion.

Radiation-Induced Neoplasia

Radiation-induced tumors are a dreaded complication from radiotherapy. Cahan et al. described the criteria for this entity in 1948. The criteria specify: (a) the tumor must arise from the irradiated field, (b) a sufficient latent period is required, (c) the tumor differs from the original neoplasm, and (d) the new tumor is rare in patients without radiation exposure³⁹. Yang et al. emphasized the need for histologic confirmation and that patients should not have genetic predispositions to secondary malignancy⁴⁰.

The latency period of new tumors ranges from one to greater than 30 years⁴¹. Meningiomas are the most common radiation-induced intracranial neoplasm overall⁴². In a study that analyzed radiation-induced neoplasms more than 20 years after radiation therapy for pituitary adenomas, sarcomas had the highest incidence, followed by gliomas and meningiomas⁴¹.

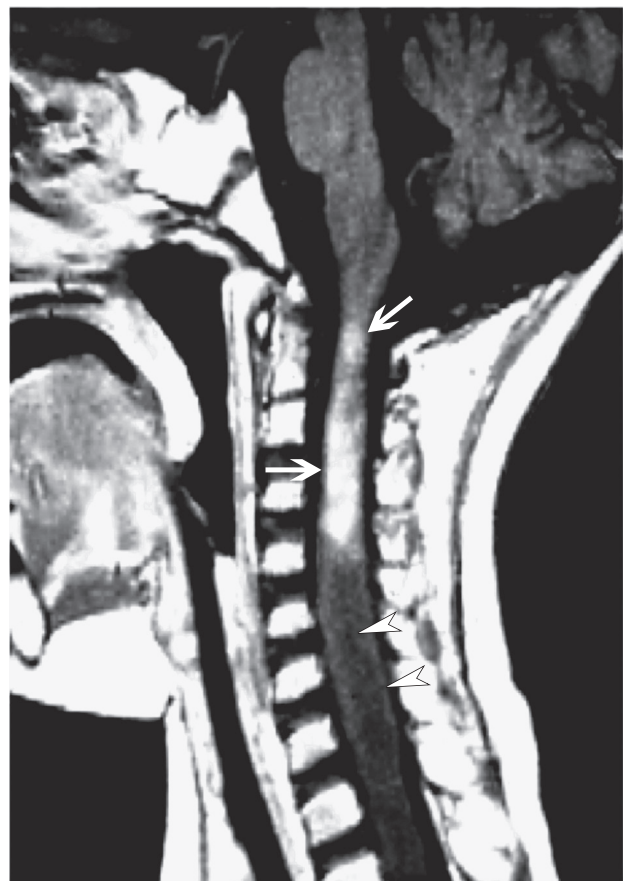


Figure 11 Disseminated necrotizing leukoencephalopathy in a 23-year-old woman after chemoradiotherapy. Sagittal contrast-enhanced T1-weighted MR image shows avid "tumor-like" enhancement of the craniocervical junction and upper cervical spinal cord (arrows). The spinal cord is edematous and shows low signal (arrowheads) inferior to the leukoencephalopathy that was compatible with a syrinx on T2-weighted imaging (not shown).

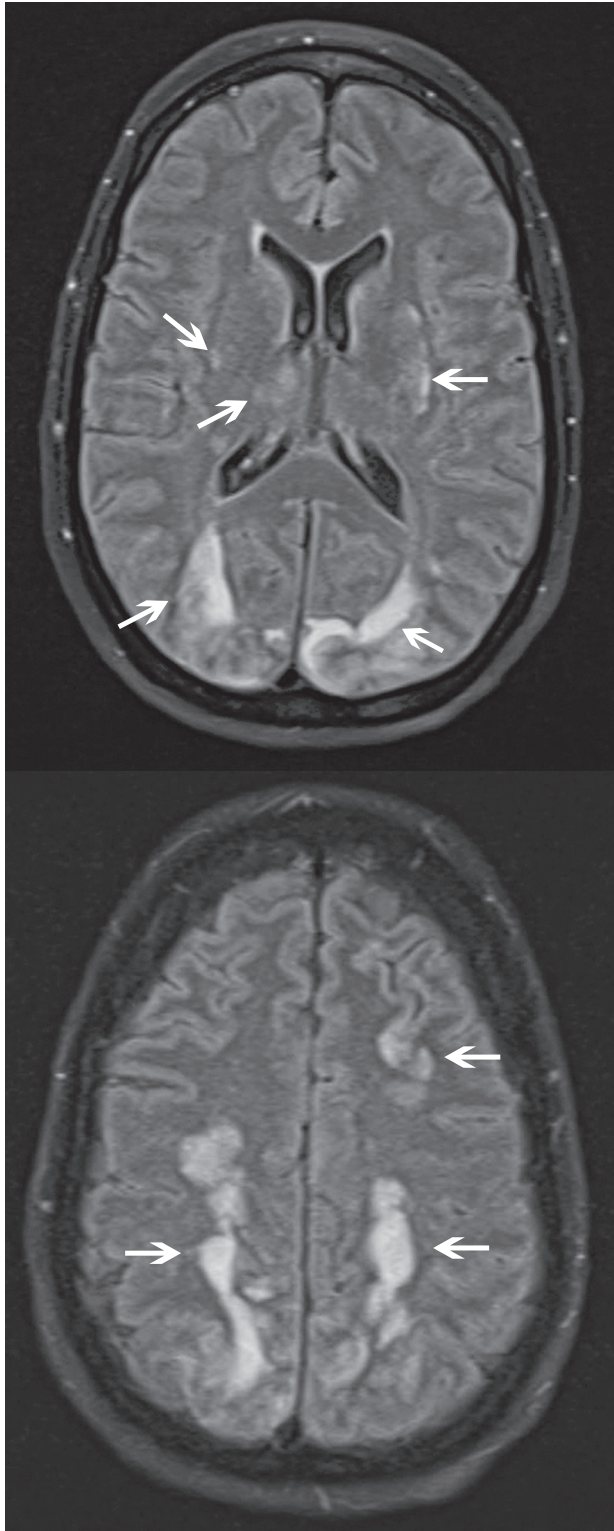


Figure 12 PRES in a 55-year-old woman after chemotherapy. A) Axial FLAIR MR image shows symmetric high signal (arrows) in the occipital lobes, thalami, and bilateral basal ganglia. B) Axial FLAIR MR image more superiorly shows symmetric high signal (arrows) in the bilateral frontal and parietal lobes. It is important to remember that PRES is not unique to brain supplied by the posterior circulation.

The reported median latency of glioma appearance is 7.0 years, 9.7 years for sarcoma, and 13.8 years for meningioma⁴³. Imaging findings of radiation-induced neoplasms are similar to native tumors (Figure 7).

White Matter Injury and Leukoencephalopathy

Radiation

Diffuse white matter injury occurs in 38–50% of patients after whole-brain radiation therapy⁴². The risk of pure radiation leukoencephalopathy is less encountered today due to increased use of localized radiation as opposed to whole-brain radiation⁴⁴. The pathogenesis of radiation-induced white matter injury varies from demyelination, gliosis, edema, to coagulation necrosis⁴⁵. Vascular injury to small and medium-sized vessels may also occur. In whole-brain or large field radiation, MR imaging demonstrates T2 hyperintense foci in the periventricular white matter that are usually symmetric. Initially, involvement is typically localized adjacent to the frontal, temporal, or occipital horns (Figure 8). As the process evolves, a confluent pattern may develop that extends to the corticomedullary junction. Focal white matter injury can also occur with radiosurgery, most commonly seen in treatment for nasopharyngeal carcinoma. MR imaging shows T2 hyperintense white matter lesions in either unilateral or bilateral temporal lobes (Figure 9). White matter lesions eventually may become contrast-enhanced lesions, in which there is interval enhancement, decrease in size, and necrosis. Complete resolution of both white matter and contrast-enhanced lesions is possible. Less frequently, cysts develop in the latest stage of temporal lobe injury and always arise from the contrast-enhanced lesions that became necrotic⁴⁶.

Chemotherapy

White matter disease can be seen with chemotherapy alone, or more often, in combination with radiation. In many cases, a mild or reversible form or leukoencephalopathy can occur acutely⁴⁴. More severe or permanent damage can be seen with methotrexate in the absence of radiation by intrathecal or intravenous administration. The mechanism of chemotherapy-induced white matter injury is poorly understood, but likely involves toxic effects on axons,

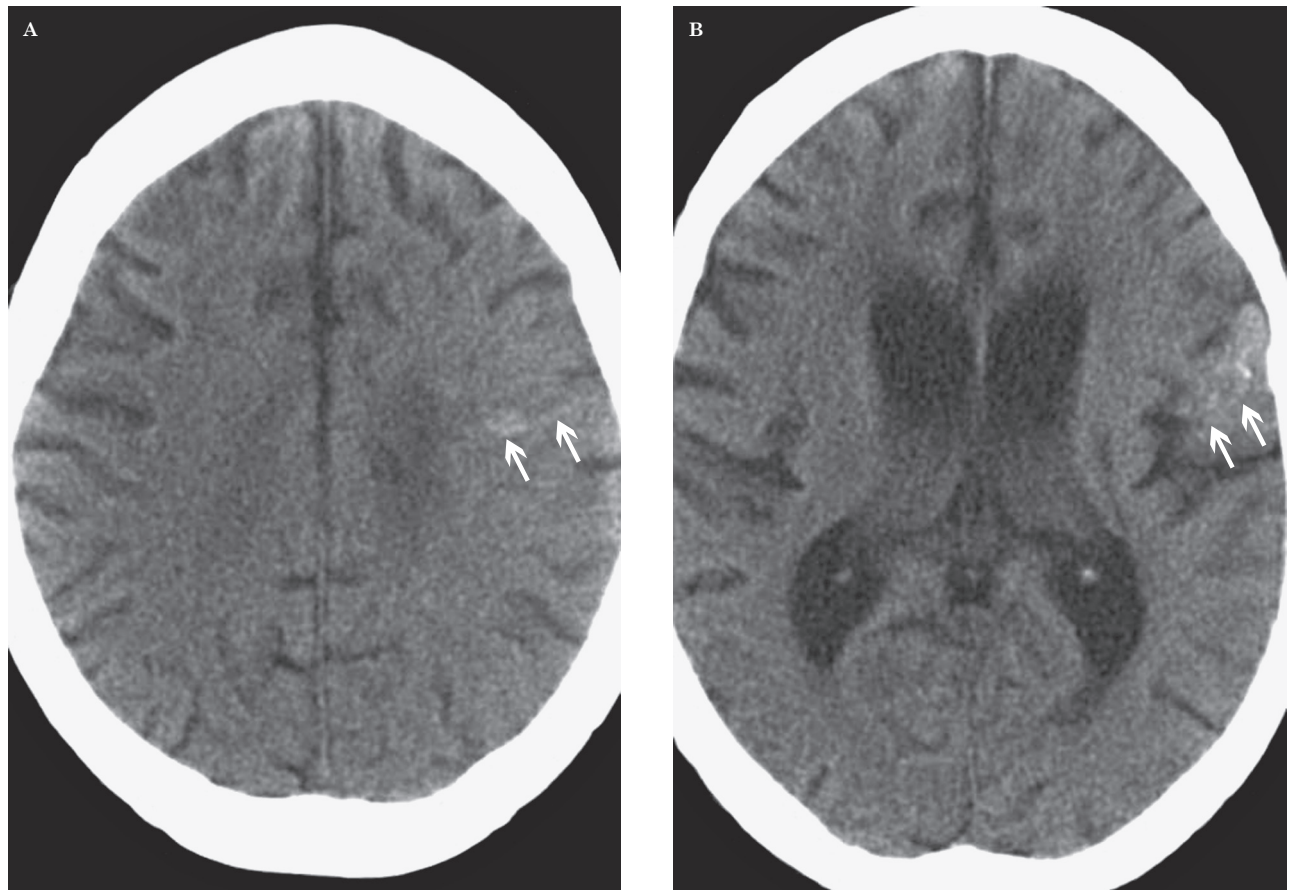


Figure 13 Mineralizing microangiopathy in a 21-year-old man with a combination of temozolomide, bevacizumab, and irradiation for anaplastic astrocytoma. A, B) Axial unenhanced CT images at the level of the centrum semiovale (A) and lateral ventricles (B) show punctate calcifications in the left frontal lobe white matter and left frontal operculum (arrows).

oligodendrocytes, progenitor cells, secondary immunologic reactions, oxidative stress, and microvascular injury⁴⁴. Imaging findings are similar to those of radiation-induced white matter injury with typical periventricular involvement. Cerebral volume loss may develop on a long-term basis. Reduced diffusion compatible with infarct is another characteristic that may be seen with acute white matter lesions (Figure 10). Infarcts may also occur with anti-angiogenic therapy. In one study, 1.9% of patients treated with bevacizumab developed ischemic infarcts⁴⁷.

Necrotizing Leukoencephalopathy

Necrotizing leukoencephalopathy is the most severe form of leukoencephalopathy. It typically occurs due to combined use of radiation and chemotherapy. Clinically, there is a shorter latency period than the other treatment-related leukoencephalopathies characterized by a rap-

idly deteriorating clinical course that is usually fatal. The pathogenesis is similar to radiation and chemotherapy-induced leukoencephalopathy, but there is a relative increase in vascular injury leading to disseminated coagulation necrosis⁴⁸. Imaging findings depict disseminated or confluent white matter lesions. “Tumor-like” enhancement and involvement of the brainstem may occur and help differentiate it from reversible milder forms of leukoencephalopathy⁴⁸; (Figure 11). Hemorrhage may be an additional finding.

Vascular-Related Pathology

Posterior Reversible Encephalopathy Syndrome

Chemotherapeutic agents such as bevacizumab and methotrexate can result in posterior reversible encephalopathy syndrome (PRES).

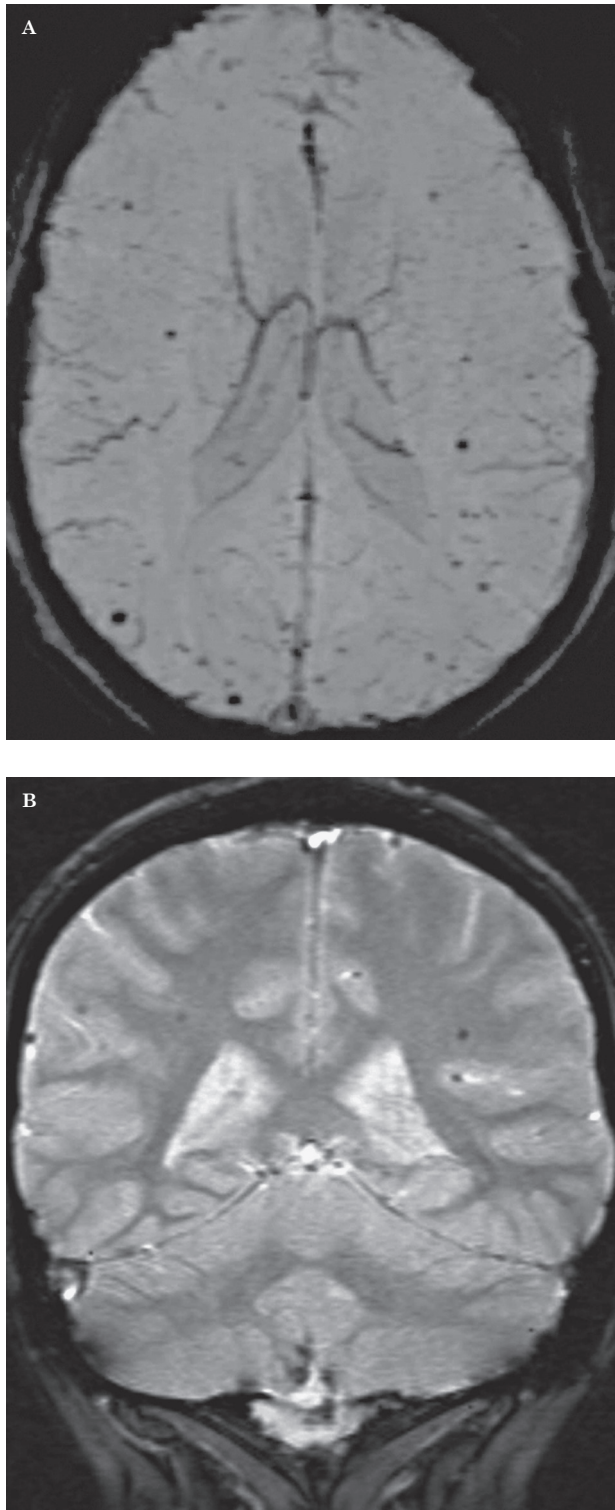


Figure 14 Radiation-induced telangiectasias in a 21-year-old man post irradiation for medulloblastoma. A) Susceptibility-weighted MR image shows numerous hypointense subcentimeter foci throughout the bilateral frontal and parietal lobes. B) Coronal gradient echo MR image shows the parietal microhemorrhages to a lesser degree. In our experience, susceptibility-weighted imaging is more sensitive than gradient echo imaging in the detection of microhemorrhages from telangiectasias.

The etiology of PRES is not completely understood, but is likely related to the lack of autoregulation of cerebral blood flow⁴⁹. Failed autoregulation leads to vasogenic edema, which is usually reversible with cessation or decrease of the chemotherapeutic dose. PRES can progress from vasogenic to cytotoxic edema and result in infarction.

Typically, PRES is bilateral, symmetric, and involves the cortical and subcortical parietal and occipital lobes. While not uncommon, asymmetric lesions may occur. Other common locations of PRES in decreasing frequency include: the posterior frontal lobe, temporal lobe, cerebellum, brainstem, thalamus, and basal ganglia⁵⁰. Given the common involvement of regions supplied by the anterior circulation, it has been suggested to remove “posterior” from the disease name⁵⁰. CT and MR imaging show low attenuation and hyperintense T2 signal in the affected areas, respectively (Figure 12). Reduced diffusion will be seen if cytotoxic edema occurs.

Mineralizing Microangiopathy

Mineralizing microangiopathy occurs most commonly with combined radiation and chemotherapy. Children are more susceptible to this entity than adults⁵¹. Histologically, mineralizing microangiopathy is characterized by calcium deposition in small vessels due to fibrinoid necrosis. On CT, there are multiple punctate calcifications in the basal ganglia, and between the basal ganglia and cortical perforating vessels (Figure 13). Cortical calcification may also be seen⁵².

Radiation-Induced Telangiectasias

Telangiectasias are another therapy-related vascular manifestation, but are unique to radiotherapy and are not seen with chemotherapy. The pathology relates to the development of telangiectasias of small capillary-sized vessels within the white matter. Radiation injury may also lead to cavernomas, which may be a variation of the same pathologic process^{53,54}. In one study of 90 children who received cranial irradiation, the frequency of radiation-induced telangiectasias was 20%⁵⁵. The latency period has been reported to range from five months to 22 years⁵⁶, with most lesions occurring after five years⁵⁵. Telangiectasias are more likely to occur in the immature brain compared to the mature brain^{56,57}. Telangiectasias may form microhemorrhages, but patients are usually

asymptomatic. MR T2-weighted or gradient echo images show hypointense foci in the cerebral white matter that are usually smaller than 10 mm in diameter⁵⁷. In our experience, susceptibility-weighted imaging is superior to gradient echo imaging to detect microhemorrhages from telangiectasias (Figure 14). These lesions can simulate amyloid angiopathy.

Conclusions

There is a wide host of treatment-related injuries secondary to radiation and chemotherapy for malignant primary glial neoplasms. CT and conventional MR imaging are the mainstay of

imaging modalities, but advanced MR imaging techniques are of growing importance and a requisite for certain post-treatment diagnoses. DSC MR perfusion is helpful to differentiate radiation necrosis and recurrent tumor—the latter giving a high rCBV. Pseudoprogression, pseudoresponse, and nonenhancing tumor are important entities that should always be considered when evaluating post-treatment brain imaging. White matter injury, varying in severity, commonly occurs after radiation and chemotherapy and is important to differentiate from tumor. It is critical for radiologists to recognize the post-treatment pathologies and their respective imaging appearances to direct future management.

References

- 1 Brandsma D, Stalpers L, Taal W, et al. Clinical features, mechanisms, and management of pseudoprogression in malignant gliomas. *Lancet Oncol.* 2008; 9 (5): 453-461.
- 2 Shah R, Vattoth S, Jacob R, et al. Radiation necrosis in the brain: imaging features and differentiation from tumor recurrence. *RadioGraphics.* 2012; 32 (5): 1343-1359.
- 3 Chamberlain MC, Glantz MJ, Chalmers L, et al. Early necrosis following concurrent Temodar and radiotherapy in patients with glioblastoma. *J Neurooncol.* 2007; 82 (1): 81-83.
- 4 Marks JE, Baglan RJ, Prasad SC, et al. Cerebral radionecrosis: incidence and risk in relation to dose, time, fractionation and volume. *Int J Radiat Oncol Biol Phys.* 1981; 7 (2): 243-252.
- 5 Leibel SA, Sheline GE. Radiation therapy for neoplasms of the brain. *J Neurosurg.* 1987; 66 (1): 1-22.
- 6 Ruben JD, Dally M, Bailey M, et al. Cerebral radiation necrosis: incidence, outcomes, and risk factors with emphasis on radiation parameters and chemotherapy. *Int J Radiat Oncol Biol Phys.* 2006; 65 (2): 499-508.
- 7 Kumar AJ, Leeds NE, Fuller GN, et al. Malignant gliomas: MR imaging spectrum of radiation therapy- and chemotherapy-induced necrosis of the brain after treatment. *Radiology.* 2000; 217 (2): 377-384.
- 8 Li YQ, Chen P, Haimovitz-Friedman A, et al. Endothelial apoptosis initiates acute blood-brain barrier disruption after ionizing radiation. *Cancer Res.* 2003; 63 (18): 5950-5956.
- 9 Moore AH, Olschowka JA, Williams JP, et al. Radiation-induced edema is dependent on cyclooxygenase 2 activity in mouse brain. *Radiat Res.* 2004; 161 (2): 153-160.
- 10 Moody DM, Bell MA, Challa VR. Features of the cerebral vascular pattern that predict vulnerability to perfusion or oxygenation deficiency: an anatomic study. *Am J Neuroradiol.* 1990; 11 (3): 431-439.
- 11 Nelson MD Jr, Gonzalez-Gomez I, Gilles FH. The search for human telencephalic ventriculofugal arteries. *Am J Neuroradiol.* 1991; 12 (2): 215-222.
- 12 Wen PY, Macdonald DR, Reardon DA, et al. Updated response assessment criteria for high-grade gliomas: response assessment in neuro-oncology working group. *J Clin Oncol.* 2010; 28 (11): 1963-1972.
- 13 Mullins ME, Barest GD, Schaefer PW, et al. Radiation necrosis versus glioma recurrence: conventional MR imaging clues to diagnosis. *Am J Neuroradiol.* 2005; 26 (8): 1967-1972.
- 14 Fatterpekar GM, Galheigo D, Narayana A, et al. Treatment-related change versus tumor recurrence in high-grade gliomas: a diagnostic conundrum—use of dynamic susceptibility contrast-enhanced (DSC) perfusion MRI. *Am J Roentgenol.* 2012; 198 (1): 19-26.
- 15 Dequesada IM, Quisling RG, Yachnis A, et al. Can standard magnetic resonance imaging reliably distinguish recurrent tumor from radiation necrosis after radiosurgery for brain metastases? A radiographic-pathological study. *Neurosurgery.* 2008; 63 (5): 898-903; discussion 904.
- 16 Chao ST, Suh JH, Raja S, et al. The sensitivity and specificity of FDG PET in distinguishing recurrent brain tumor from radionecrosis in patients treated with stereotactic radiosurgery. *Int J Cancer.* 2001; 96 (3): 191-197.
- 17 Ricci PE, Karis JP, Heiserman JE, et al. Differentiating recurrent tumor from radiation necrosis: time for re-evaluation of positron emission tomography? *Am J Neuroradiol.* 1998; 19 (3): 407-413.
- 18 Hazle JD, Jackson EF, Schomer DF, et al. Dynamic imaging of intracranial lesions using fast spin-echo imaging: differentiation of brain tumors and treatment effects. *J Magn Reson Imaging.* 1997; 7 (6): 1084-1093.
- 19 Fink JR, Carr RB, Matsusue E, et al. Comparison of 3 Tesla proton MR spectroscopy, MR perfusion and MR diffusion for distinguishing glioma recurrence from posttreatment effects. *J Magn Reson Imaging.* 2012; 35 (1): 56-63.
- 20 Barajas RF Jr, Chang JS, Segal M, et al. Differentiation of recurrent glioblastoma multiforme from radiation necrosis after external beam radiation therapy with dynamic susceptibility-weighted contrast-enhanced perfusion MR imaging. *Radiology.* 2009; 253 (2): 486-496.
- 21 Barajas RF, Chang JS, Sneed PK, et al. Distinguishing recurrent intra-axial metastatic tumor from radiation necrosis following gamma knife radiosurgery using dynamic susceptibility-weighted contrast-enhanced perfusion MR imaging. *Am J Neuroradiol.* 2009; 30 (2): 367-372.
- 22 Sugahara T, Korogi Y, Tomiguchi S, et al. Posttherapeutic intraaxial brain tumor: the value of perfusion-sensitive contrast-enhanced MR imaging for differentiating tumor recurrence from nonneoplastic contrast-enhancing tissue. *Am J Neuroradiol.* 2000; 21 (5): 901-909.

- 23 Hu LS, Baxter LC, Smith KA, et al. Relative cerebral blood volume values to differentiate highgrade glioma recurrence from posttreatment radiation effect: direct correlation between image-guided tissue histopathology and localized dynamic susceptibility-weighted contrast-enhanced perfusion MR imaging measurements. *Am J Neuroradiol.* 2009; 30 (3): 552-558.
- 24 Warmuth C, Gunther M, Zimmer C. Quantification of blood flow in brain tumors: comparison of arterial spin labeling and dynamic susceptibility-weighted contrast-enhanced MR imaging. *Radiology.* 2003; 228 (2): 523-532.
- 25 Sundgren PC. MR spectroscopy in radiation injury. *Am J Neuroradiol.* 2009; 30 (8): 1469-1476.
- 26 Zeng QS, Li CF, Zhang K, et al. Multivoxel 3D proton MR spectroscopy in the distinction of recurrent glioma from radiation injury. *J Neurooncol.* 2007; 84 (1): 63-69.
- 27 Hein PA, Eskey CJ, Dunn JF, et al. Diffusion-weighted imaging in the follow up of treated high-grade gliomas: tumor recurrence versus radiation injury. *Am J Neuro-radiol.* 2004; 25 (2): 201-209.
- 28 Sundgren PC, Fan X, Weybright P, et al. Differentiation of recurrent brain tumor versus radiation injury using diffusion tensor imaging in patients with new contrast. *Magn Reson Imaging.* 2006; 24 (9): 1131-1142.
- 29 Pope WB, Kim HJ, Huo J, et al. Recurrent glioblastoma multiforme: ADC histogram analysis predicts response to bevacizumab treatment. *Radiology.* 2009; 252 (1): 182-189.
- 30 Macdonald DR, Cascino TL, Schold SC Jr, et al. Response criteria for phase II studies of supratentorial malignant glioma. *J Clin Oncol.* 1990; 8 (7): 1277-1280.
- 31 Taal W, Brandsma D, de Bruin HG, et al. Incidence of early pseudo-progression in a cohort of malignant glioma patients treated with chemoradiation with temozolomide. *Cancer.* 2008; 113 (2): 405-410.
- 32 Brandes AA, Franceschi E, Tosoni A, et al. MGMT promoter methylation status can predict the incidence and outcome of pseudoprogression after concomitant radiochemotherapy in newly diagnosed glioblastoma patients. *J Clin Oncol.* 2008; 26 (13): 2192-2197.
- 33 Clarke JL, Chang S. Pseudoprogression and pseudoresponse: challenges in brain tumor imaging. *Curr Neurol Neurosci Rep.* 2009; 9 (3): 241-246.
- 34 Hygino da Cruz LC Jr, Rodriguez I, Domingues RC, et al. Pseudoprogression and pseudoresponse: imaging challenges in the assessment of posttreatment glioma. *Am J Neuroradiol.* 2011; 32 (11): 1978-1985.
- 35 Mangla R, Singh G, Ziegelitz D, et al. Changes in relative cerebral blood volume 1 month after radiation-temozolomide therapy can help predict overall survival in patients with glioblastoma. *Radiology.* 2010; 256 (2): 575-584.
- 36 Yamasaki F, Kurisu K, Aoki T, et al. Advantages of high b-value diffusion-weighted imaging to diagnose pseudo-responses in patients with recurrent glioma after bevacizumab treatment. *Eur J Radiol.* 2012; 81 (10): 2805-2810.
- 37 Thompson EM, Frenkel EP, Neuwelt EA. The paradoxical effect of bevacizumab in the therapy of malignant gliomas. *Neurology.* 2011; 76 (1): 87-93.
- 38 Jain RK, Duda DG, Willett CG, et al. Biomarkers of response and resistance to antiangiogenic therapy. *Nat Rev Clin Oncol.* 2009; 6 (6): 327-338.
- 39 Cahan WG, Woodard HQ, Higinbotham NL, et al. Sarcoma arising in irradiated bone: report of eleven cases. *Cancer.* 1948; 1 (1): 3-29.
- 40 Yang SY, Wang KC, Cho BK, et al. Radiation-induced cerebellar glioblastoma at the site of a treated medulloblastoma: case report. *J Neurosurg.* 2005; 102 (Suppl 4): 417-422.
- 41 Wu-Chen WY, Jacobs DA, Volpe NJ, et al. Intracranial malignancies occurring more than 20 years after radiation therapy for pituitary adenoma. *J Neuroophthal-mol.* 2009; 29 (4): 289-295.
- 42 Rabin BM, Meyer JR, Berlin JW, et al. Radiation-induced changes in the central nervous system and head and neck. *RadioGraphics.* 1996; 16 (5): 1055-1072.
- 43 Brada M, Ford D, Ashley S, et al. Risk of second brain tumour after conservative surgery and radiotherapy for pituitary adenoma. *BMJ.* 1992; 304 (6838): 1343-1346.
- 44 Perry A, Schmidt RE. Cancer therapy-associated CNS neuropathology: An update and review of the literature. *Acta Neuropathol.* 2006; 111 (3): 197-212.
- 45 Chan YL, Leung SF, King AD, et al. Late radiation injury to the temporal lobes: morphologic evaluation at MR imaging. *Radiology.* 1999; 213 (3): 800-807.
- 46 Wang YX, King AD, Zhou H, et al. Evolution of radiation-induced brain injury: MR imaging-based study. *Radiology.* 2010; 254 (1): 210-218.
- 47 Fraum TJ, Kreisl TN, Sul J, et al. Ischemic stroke and intracranial hemorrhage in glioma patients on antiangiogenic therapy. *J Neurooncol.* 2011; 105 (2): 281-289.
- 48 Raghavendra S, Nair MD, Chemmanam T, et al. Disseminated necrotizing leukoencephalopathy following low-dose oral methotrexate. *Eur J Neurol.* 2007; 14 (3): 309-314.
- 49 Wu Q, Marescaux C, Wolff V, et al. Tacrolimus-associated posterior reversible encephalopathy syndrome after solid organ transplantation. *Eur Neurol.* 2010; 64 (3): 169-177.
- 50 McKinney AM, Short J, Truwit CL, et al. Posterior reversible encephalopathy syndrome: incidence of atypical regions of involvement and imaging findings. *Am J Roentgenol.* 2007; 189 (4): 904-912.
- 51 Pruzincová L, Steno J, Srbecký M, et al. MR imaging of late radiation therapy- and chemotherapy-induced injury: a pictorial essay. *Eur Radiol.* 2009; 19 (11): 2716-2727.
- 52 Valk PE, Dillon WP. Radiation injury of the brain. *Am J Neuroradiol.* 1991; 12 (1): 45-62.
- 53 Larson JJ, Ball WS, Bove KE, et al. Formation of intracerebral cavernous malformations after radiation treatment for central nervous system neoplasia in children. *J Neurosurg.* 1998; 88 (1): 51-56.
- 54 Rigamonti D, Drayer BP, Johnson PC, et al. The MRI appearance of cavernous malformations (angiomas). *J Neurosurg.* 1987; 67 (4): 518-524.
- 55 Koike S, Aida N, Hata M, et al. Asymptomatic radiation-induced telangiectasia in children after cranial irradiation: frequency, latency, and dose relation. *Radiology.* 2004; 230 (1): 93-99.
- 56 Gaensler EHL, Dillon WP, Edwards MS, et al. Radiation-induced telangiectasia in the brain simulates cryptic vascular malformations at MR imaging. *Radiology.* 1994; 193 (3): 629-636.
- 57 Oi S, Kokunai T, Ijichi A, et al. Radiation induced brain damage in children: histologic analysis of sequential tissue changes in 34 autopsies. *Neurol Med Chir (Tokyo).* 1990; 30 (1): 36-42.

Mark D. Mamlouk, MD
University of California, Irvine,
101 The City Drive South, Route 140
Orange, CA 92868
Tel.: 714-456-6579
Fax: 714-740-5013
E-mail: mamlouk@gmail.com